Anal Bioanal Chem (2011) 399:1021–1029
DOI 10.1007/s00216-010-4419-8

ORIGINAL PAPER

Multifunctional nanoparticles as simulants for a gravimetric immunoassay

Scott A. Miller · Leslie A. Hiatt · Robert G. Keil · David W. Wright · David E. Cliffel

Received: 24 September 2010 / Revised: 28 October 2010 / Accepted: 2 November 2010 / Published online: 26 November 2010

Abstract Immunoassays are important tools for the rapid detection and identification of pathogens, both clinically and in the research laboratory. An immunoassay with the potential for the detection of influenza was developed and tested using hemagglutinin (HA), a commonly studied glycoprotein found on the surface of influenza virions. Gold nanoparticles were synthesized, which present multiple peptide epitopes, including the HA epitope, in order to increase the gravimetric response achieved with the use of a QCM immunosensor for influenza. Specifically, epitopes associated with HA and FLAG peptides were affixed to gold nanoparticles by a six-mer PEG spacer between the epitope and the terminal cysteine. The PEG spacer was shown to enhance the probability for interaction with antibodies by increasing the distance the epitope extends from the gold surface. These nanoparticles were characterized using thermogravimetric analysis, transmission electron microscopy, matrix-assisted laser desorption/ionization-time of flight, and ^{1}H nuclear magnetic resonance analysis. Anti-FLAG and anti-HA antibodies were adhered to the surface of a QCM, and the response of each antibody upon exposure to HA, FLAG, and dual functionalized nanoparticles was compared with binding of Au–tiopronin nanoparticles and H5 HA proteins from influenza virus (H5N1). Results demonstrate that the immunoassay was capable of differentiating between nanoparticles presenting orthogonal epitopes in real-time with minimal nonspecific binding. The detection of H5 HA protein demonstrates the logical extension of using these nanoparticle mimics as a safe positive control in the detection of influenza, making this a vital step in improving influenza detection methodology.

Keywords Immunosensor · Nanoparticle · Quartz crystal microbalance · Viral simulant · ELISA · Influenza simulant · FLAG · Hemagglutinin · Epitope · PEG linkage · H5N1

Electronic supplementary material The online version of this article (doi:10.1007/s00216-010-4419-8) contains supplementary material, which is available to authorized users.

S. A. Miller · L. A. Hiatt · R. G. Keil · D. W. Wright (✉) · D. E. Cliffel (✉)
Department of Chemistry, Vanderbilt University,
7330 Stevenson Center, VU Station B 351822,
Nashville, TN 37235-1822, USA
e-mail: david.wright@vanderbilt.edu

D. E. Cliffel
e-mail: d.cliffel@vanderbilt.edu

Present Address:
S. A. Miller
Department of Chemistry, University of South Alabama,
Mobile, AL 36688, USA

Present Address:
R. G. Keil
Department of Chemistry, University of Dayton,
Dayton, OH 45469, USA

Introduction

Viruses are the smallest form of life on earth with the ability to replicate and spread within living cells [1]. As they pass from cell to cell, they adapt to evade host immunity and spread disease, creating some of the worst pandemics in history [2]. Improving diagnostics for viruses, such as influenza, would help slow the spread of infection in the event of an emerging virus. It is known that even with reassortment, a common viral defense mechanism, the majority of anti-hemagglutinin (anti-HA) antibodies recognize a specific nine amino acid sequence within the epitope, AYDPVDYPY, which has been the focus of many assays to

improve the detection of influenza [3]. Using this immunodominant sequence for the HA epitope, the influenza epitope can be mimicked with a functionalized nanoparticle yielding a comparable affinity to the linear peptide [4]. Another virus, Ebola, has also been effectively mimicked with a monolayer-protected cluster (MPC) through functionalization of the MPC with the antigenic determinant of the Ebola glycoprotein [5]. Integrating biology and materials chemistry using biomimicry in this way has allowed materials chemistry the opportunity to improve current diagnostic treatments, techniques, and limits of detection, but further improvements are still yet to be made [6].

The utilization of immuno-molecular recognition in the assembly of nanoscale sensors has applications in medical diagnosis, treatment, and the understanding of diseases [7]. Enzyme-linked immunosorbent assay (ELISA) is widely utilized in clinics and hospitals as an initial screening for several infectious diseases. While ELISA can be effectively employed in laboratory settings for common infectious agents, several obstacles inhibit the adaptation of this standard clinical assay to portable or select agent detection schemes. Unfortunately, pathogenic agent detection requires calibration with irradiated or otherwise attenuated samples of the organism. This requirement limits the widespread use of immunosensor diagnostics because of the scarcity of these agents and the logistic difficulty in safe transportation to remote locations. Recent cases like the development of meningitis and tularemia infections in researchers who were working with the causative agents of these diseases alert scientists to the hazards accompanying work with live calibrants [8]. The possibility of exposure and high cost are enough to warrant investigation into a safer positive control for these disease detection assays and devices. Without a positive control, the operational status of the sensor cannot be determined. Thus, the development of a nanoparticle mimic would be a safer alternative to current methodology and could be extended to address the needs of other assays that incorporate well-defined epitopes.

Many traditional clinical assays lack the ability for electronic adaptation and timely results. The need exists for rapid, sensitive, and inexpensive methods that could be utilized in clinical settings [9]. Therefore, the rapid real-time quantification of a QCM has been combined with the selectivity of monoclonal antibodies to create an immunosensor for evaluation of the multifunctional nanoparticles. The use of a QCM for immunological detection has been demonstrated previously, where it has been shown to detect *Staphylococcus epidermidis* in clinical samples using nanoparticle amplification [10], SARS virus in sputum samples [11], plant pathogens [12], an antigenic mimic of Ebola [5], and influenza A and B from nasal washes [13]. In QCM assays, nanoparticles have enabled simultaneous parallel detection and amplification for gravimetry, thus lowering the limit of detection [6, 14–17]. A QCM-based sensor with a nanoparticle control would allow for the simultaneous rapid and accurate analysis of multiple viral or biological hazards, without posing a safety or health threat. The work reported here builds on this previous work and addresses the specificity of detection of antibody–antigen binding at the QCM using polyepitope-functionalized gold nanoparticles.

Gold nanoparticles have favorable characteristics for their use as the basis for multifunctional microorganism simulants [18]. Nanoparticle size, shape, and capacity for surface modifications, based on chemical characteristics and environments, make the use of nanoparticles advantageous for detection, discovery, and diagnosis [7, 19]. Previous studies have shown that nanoparticles are capable of accepting a wide array of functional molecules via the Au-thiol bonds at the interface of the ligand and particle [20]. Since the physical and chemical properties of nanoparticles are dependent upon size [6], the gold nanoparticles can be customized to simulate the variability in pathogen size. MPCs in this work had an average diameter of 2.6± 0.6 nm. Influenza virions vary in size, normally around 100 nm in diameter, but smaller nanoparticles were chosen in this study since they have a larger surface area to volume ratio and therefore increase the ratio of possible antigen presentation to gold core [21]. These nanoparticles were polyfunctionalized to increase the presentation of the nanoparticle epitope to the antibody. Previous studies have found multivalent ligand attachment to gold nanoparticles enhances the affinity measured in binding studies [22, 23]. The selectivity of antibody sensors for functionalized MPCs has been examined using two orthogonal epitopes: FLAG and HA. The FLAG epitope is a biological peptide sequence commonly used for identification of proteins in biological samples [24]. HA- and FLAG-functionalized MPCs can be used as a synthetic simulant and negative control for the HA epitope of the influenza virus [25, 26]. The binding of these nanoparticles was also compared with binding of negative-control Au–tiopronin nanoparticles and an authentic sample of H5 HA proteins from influenza virus (H5N1). The simulants work as safe controls whose application could be extended to address various pathological threats, in which using attenuated controls is problematic.

Experimental

Chemicals Gold shot was purchased from precious metal vendors (Canadian Maple Leaf, 99.99%) and was initially converted to $HAuCl_4 \cdot 3\ H_2O$ by boiling Au^0 in HCl/HNO_3 solution [27]. *N*-(2-Mercaptopropionyl)-glycine (tiopronin, reagent grade), bovine serum albumin (BSA, fraction V, 96%), and sodium phosphate (monobasic, reagent grade) were purchased from Sigma. Other chemicals were

obtained as follows: protein G was purchased from Southern Biotech, Fmoc-dPEG-COOH from Quanta Biodesign, anti-FLAG mouse monoclonal antibody from Stratagene, and anti-HA mouse monoclonal antibody from the Vanderbilt Molecular Recognition Core facility. The following reagent was obtained through the NIH Biodefense and Emerging Infections Research Resources Repository, NIAID, NIH: H5 HA protein from influenza virus, A/Hong Kong/156/97 (H5N1), recombinant from baculovirus, and NR-652 (56 kDa) [28]. Analytical grade solvents for nuclear magnetic resonance (NMR) were obtained from Cambridge Isotope Laboratories, and water was purified using a Modulab Water Systems unit (~18 MΩ/cm). Buffers were prepared according to standard laboratory procedure. Other chemicals were reagent grade and used as received.

MPC synthesis and characterization Gold–tiopronin-protected MPCs were synthesized as previously described [29–31]. Briefly, tiopronin-protected gold nanoparticles were synthesized by dissolving tiopronin and $HAuCl_4 \cdot 3H_2O$ (3:1) into a MeOH/acetic acid solution (6:1). The reaction was stirred for 30 min and then cooled in an ice bath. $NaBH_4$ was then added in 10× molar excess of gold. Reaction product was stirred for 1 h. The solvent was removed under vacuum, and the pH was lowered to 1 with concentrated HCl. Reaction product purification by dialysis with cellulose ester membranes (Spectra/Por CE, MWCO= 10,000) removed any excess tiopronin. Average particle diameter was determined by transmission electron microscopy (TEM). TEM images were taken on a Phillips CM20 instrument after applying aqueous MPC samples to Formvar-coated 200-mesh copper grids (Ted Pella). The microscope operated at 200 keV with magnification in the range ×150–750,000. Thermogravimetric analysis (TGA) was performed with a TGA 1000 (Instrument Specialists, Inc.) to calculate Au–tiopronin stoichiometry. From TEM and TGA data, the nanoparticle size and Au–tiopronin stoichiometry were obtained. MPCs used in the following experiments had an average diameter of 2.6±0.6 nm and a base composition of $Au_{544}Tiop_{204}$ (140.4 kDa), calculated from TEM and TGA data (at 650 °C), respectively (Electronic Supplementary Material Figs. S1, S2, and S4) [32–34].

Peptide synthesis and characterization The FLAG and HA epitopes were synthesized with standard 9-fluorenylmethoxycarbonyl (Fmoc protocols on a solid resin support) [35, 36]. Epitope sequences were modified with a linker region comprised of a discrete polyethylene glycol (PEG, purchased as Fmoc-dPEG™ from Quanta Biodesign) and a C-terminal cysteine. PEG was added to attenuate nonspecific binding, while the C-terminal cysteine provided a thiol linkage to the gold surface. PEG formed the link between the cysteine and the rest of the peptide, HA-PEG-C for example. After initial MPC, studies performed without the PEG linker were found to have no binding; all future studies incorporated this linkage. The notations HA-Au, HA-FLAG-Au, and FLAG-Au are assumed to include the incorporation of this linkage. Epitope antigens HA (AYDPVDYPY-$(PEG)_6$-C, 1562.6 Da) and FLAG (KDDDDKYD-$(PEG)_6$-C, 1451.5 Da) were synthesized on an Apex 396 (Advanced Chemtech) equipped with a 96-well reaction block capable of vortex mixing. 2-Chlorotrityl resin was swollen in dichloromethane (Fisher) prior to synthesis [37]. Fmoc amino acids (Synpep) and Fmoc-$dPEG_6$ acid (Quanta Biodesign) were coupled using *O*-benzotriazole-*N*,*N*,*N*′,*N*′-tetramethyl-uronium-hexafluoro-phosphate (HBTU, 5 eq with respect to resin, Synpep), 1-hydroxybenzatriazole (Hobt, 5 eq, Synpep), and *N*,*N*-diisopropylethylamine (DIEA, 10 eq, Advanced Chemtech) in *N*,*N*,-dimethylformamide (DMF, Fisher). Peptides were cleaved with 90% (*v*/*v*) trifluoroacetic acid, 5% anisole (Sigma), 3% thioanisole (Sigma), and 2% ethanedithiol (Sigma). Final purification was performed on a Waters C18 semi-prep RP HPLC column using a water (0.05% trifluoroacetic acid and acetonitrile) gradient. Peptide identity was confirmed via matrix-assisted laser desorption/ionization-time of flight analysis.

Place exchange Place exchange reactions between tiopronin-MPCs and thiolate-containing peptides, HA and FLAG, followed a method similar to Hostetler et al. [18, 38, 39] and assumes that epitope–tiopronin S_N2 place exchange is one for one. While it has been shown by ^1H NMR that the interchange of ligands is 1:1, the final ratio of the original ligand to exchanged ligand depends on ligand length, concentration of entering and exiting ligands, as well as the placement of the ligand (vertice, edge, or terrace) on the surface of the cluster [18, 38]. It should also be noted that the reported ratio will be an average exchanged ratio calculated from ^1H NMR, as the dispersity of MPC size will cause variations in the exact number of exchanged ligands on each cluster [18]. With the X-ray diffraction identification [40] of staple motifs, which are composed of one Au(I) and two thiolates, as part of the capping structure on gold–thiolate nanoparticles, place exchange must insert the new thiolate into the existing staples at the same time as the previous thiolate is lost in the S_N2 mechanism. Tiopronin MPCs were co-dissolved in DI water with free thiolated epitope (1:10). If necessary to aid the solvation of the epitopes into water, the epitopes were first dissolved into ethanol. The place exchange reaction took only one night for the exchange of a single epitope, while requiring 3 days for the exchange of two epitopes simultaneously. Solutions were dialyzed at room temperature for approximately 3 days as previously described and

then dried under air [29]. The epitope composition of the MPCs was determined by TGA and ^{1}H NMR analysis (Electronic Supplementary Material Figs. S2 and S3).

Nuclear magnetic resonance ^{1}H NMR experiments were run at 300 MHz on a Bruker DPX-300 instrument with 5 s relaxation times. Samples were dissolved in D_2O. The extent of place substitution of tiopronin by epitope on gold nanoparticles was determined by ^{1}H NMR, using methods previously described [18, 31].

Enzyme-linked immunosorbent assay Initial tests to determine whether the functionalized nanoparticles were suitable as both a viral simulant and a synthetic calibrant were performed using ELISAs. Positive activity was established by adhering gold nanoparticles (250–500 ng/per well) with a variety of functionalities (Au–Tiop, HA-Au, FLAG-Au, and HA-FLAG-Au) to a 96-well Immulon 2HB plate. Buffer and free peptides (25 μg/well) were plated and tested in a similar fashion. Blocking was achieved with BSA (1 mg/mL), followed by exposure to either anti-FLAG or anti-HA primary antibodies (at recommended dilutions, monoclonal mouse). Horseradish peroxidase linked anti-mouse antibodies (1:5000 dilution) were then added, followed by exposure to tetramethylbenzidine (TMB, Sigma) substrate solution. The reaction was halted with 2 M H_2SO_4, and the plates were read at 450 nm (BioTek Synergy HT plate reader).

Immunosensor assembly The immunosensor was assembled on a 5-MHz AT-cut quartz crystal. Before assembly, the gold electrode was triple cleaned in piranha, and then received a final ethanol or acetone rinse and dried in a stream of N_2 (grams). The quartz crystal was then mounted in a flow cell holder, rinsed with phosphate buffer (PB, 50 mM phosphate, pH 7.2), and brought to resonant frequency at room temperature. For the work described herein, a Stanford Research Systems quartz crystal microbalance model 200, which measures both frequency and resistance, was used. Solutions were passed through the cell at a flow rate of 28 μL/min controlled by a Masterflex peristaltic pump. The sequence for biosensor assembly was protein G (20 μg/mL, 10 min), BSA (1 mg/mL, 5 min), antibody (20 μg/mL, 16 min), and viral simulant (500 μg/mL, 11 min) all in PB. The nanoparticles were filtered prior to use with a 0.22-μm filter from Millipore. The crystal was washed for a minimum of 10 min with PB between each step. Deposition of protein G allowed for the immobilization of the Fc region of anti-HA and anti-FLAG antibodies. The binding of non-functionalized Au–tiop nanoparticles (500 μg/mL, 11 min) with anti-HA antibodies was used as a negative control and as a test for nonspecific binding. Positive control was established utilizing anti-HA's recognition of recombinant H5 HA protein (5 μg/mL, 10 min).

The adsorbance of each of these molecules resulted in changes in both frequency and resistance. The bound analyte mass is proportional to changes in the oscillation frequency of the quartz crystal as described by the Sauerbrey equation (Eq. 1), where Δf is the change in frequency, C_f is the known sensitivity factor of a 5-MHz crystal (56.6 Hz cm^2 μg^{-1}), and Δm is the change in mass [41]:

$$\Delta f = -C_f \Delta m. \quad (1)$$

In addition to mass, the frequency of the crystal is also dependent on the density and viscosity of the contact medium, a consequence of the solution's resistance to crystal oscillation [42]. The crystal frequency and resistance were recorded during the QCM experiments to allow for corrections to be made for solution resistance, following the work of Kanazawa and Martin [43–45], which modifies the standard Sauerbrey equation to:

$$\Delta f_{\text{Mass load}} = \Delta f_{\text{Measured}} + \Delta f_{\text{Resistance}} = -C_f \Delta m. \quad (2)$$

Frequency change for solution resistance is nominally −2.464 Hz/Ω given an active crystal surface area equal to 0.40 cm^2 per sucrose calibrations similar to work reported previously [32]. The resulting change in mass is therefore a combination of changes in resistance and frequency, while taking into account solution resistance. The QCM results corroborated results from the ELISAs.

Results and discussion

In the development of a synthetic positive control for this influenza immunoassay, functionalized gold MPCs were synthesized and characterized. TEM analysis of the tiopronin–gold nanoparticles (Au–tiop) resulted in an average cluster size of 2.6±0.6 nm, with a range from 1.5 to 4 nm (Electronic Supplementary Material Fig. S1). The TGA tiopronin MPC mass loss equaled 37.9% and yielded a 2.67 Au:Tiop stoichiometric ratio for the nanoparticles assuming the loss of the Au(I)–thiolate staples (Electronic Supplementary Material Figs. S2 and S4). The assumption of the loss of the Au(I)–thiolate staples is justified by the observation of gold–thiolate compounds upon thermal decomposition in a mass spectrometer [46]. The average number of gold atoms calculated per cluster equaled 544 atoms. Combining the TEM and TGA yields a calculated empirical formula $Au_{544}Tiop_{204}$ for the 2.6-nm diameter particle. Following place exchange of epitope(s) for tiopronin, the epitope loading was determined through ^{1}H

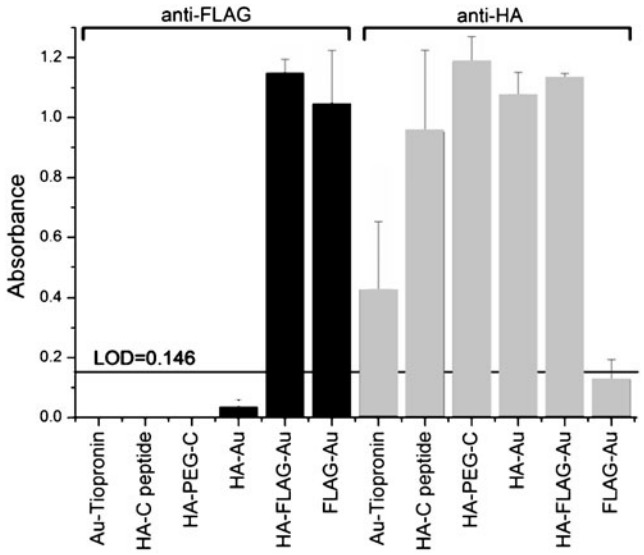

Fig. 1 Measured absorbance at 450 nm for the interactions of peptides and functionalized gold nanoparticles with FLAG and HA antibodies demonstrating normal and orthogonal antigen–antibody binding (n=3 for all data points)

NMR (Electronic Supplementary Material Fig. S3). The epitopes HA and FLAG each contain an exclusive amino acid whose proton signal occurs at a unique location in the ^{1}H NMR spectrum. Specifically, valine (V) is unique to the FLAG epitope and lysine (K) to the HA epitope. Tyrosine (Y) is common to both epitopes, but occurs in different stoichiometric ratios. The integrated resonance for each functionalized nanoparticle can be compared with that for nanoparticles protected solely with tiopronin to determine the average epitope stoichiometry of the nanoparticles. Peaks used for quantification consisted of signals at 1.2 ppm (V, 2 CH_3), 1.45 ppm (tiopronin, CH_3), 2.90 ppm (K, 2 ε-CH_2), 6.75 ppm (Y, δ-CH), and 7.05 ppm (Y, ε-CH). The ^{1}H NMR data allowed for the nanoparticle stoichiometry to be calculated. The HA and FLAG epitope compositions and molecular weight are (a) $Au_{544}Tiop_{153}FLAG_{30}HA_{22}$, 210.0 kDa; (b) $Au_{544}Tiop_{191}HA_{13}$, 158.6 kDa; and (c) $Au_{544}Tiop_{190}FLAG_{14}$, 158.5 kDa (Electronic Supplementary Material Fig. S4).

The ELISA results confirmed specificity of the functionalized gold nanoparticles to the anti-HA and anti-FLAG antibodies (Fig. 1). Evidence of cross reactivity between the gold nanoparticles presenting both peptides and both antibodies corroborates with QCM data. HA-FLAG-Au and FLAG-Au were detected with the anti-FLAG antibodies, while HA peptides and HA-Au were not. Correspondingly, HA peptides, HA-Au, and HA-FLAG-Au were recognized by anti-HA, while FLAG-Au was not. The LOD was calculated to be 0.146 OD using the average absorbance of wells incorporating buffer only in the initial step, which served as a negative control. The gold particles displaying only tiopronin (Au–tiopronin) appeared to nonspecifically bind with anti-HA. Nonspecific binding could be reduced in ELISAs with the use of higher concentrations of BSA or with the use of more stringent rinsing protocols, such as the use of Tween 20, a nonionic surfactant, between steps, which might also remove bound particles and lower the sensitivity of these assays [47]. MPCs functionalized without the PEG linker between the epitope and the cysteine linkage showed no binding with their respective antibodies in either ELISA or QCM experiments, but once the PEG link was incorporated into the mimic's

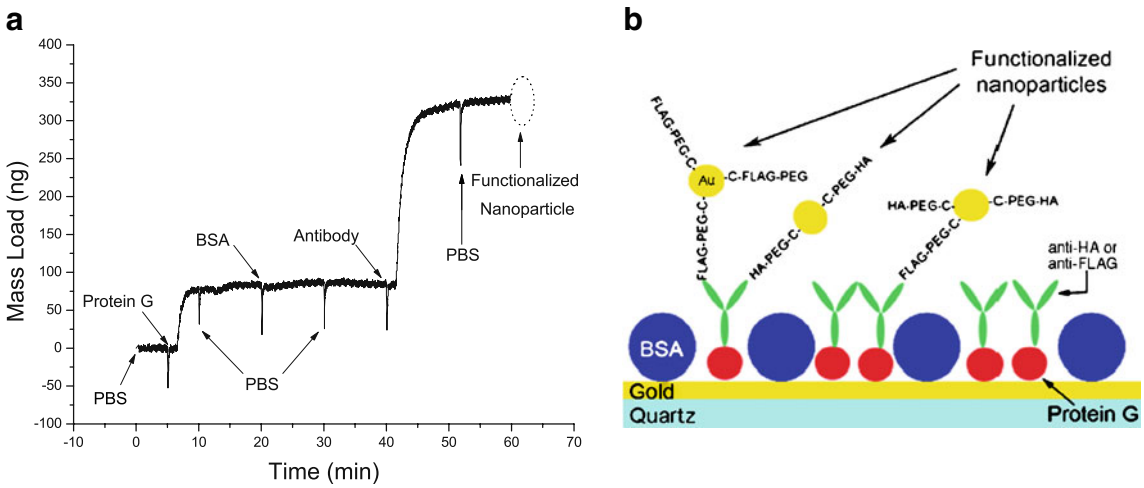

Fig. 2 **a** QCM immunosensor assembly sequence is recorded. Solutions are pumped over the crystal in this order: protein G, bovine serum albumin (BSA), antibody (HA or FLAG), and functionalized nanoparticle addition depicted. Phosphate buffer (PB, pH 7.2) flows at the beginning of each experiment and between additions as indicated to establish and re-establish baseline levels. This figure is a representative experiment showing the typical binding seen during the course of an experiment. **b** A schematic of the binding occurring on the sensor is shown. Refer to Table 1 to see average binding for all experiments

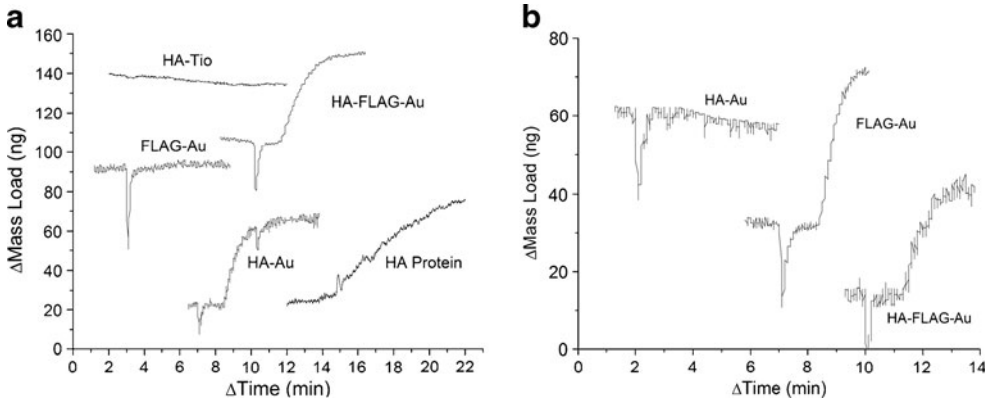

Fig. 3 Functionalized gold MPC binding measured with a QCM. Response to functionalized gold nanoparticles at room temperature from eight different experiments is shown. The data was normalized in time and in mass load, keeping the relative changes the same as the original data, for aesthetic purposed in combining all the data on two graphs. The responses were generated using (**a**) anti-HA and (**b**) anti-FLAG antibodies. An increase in mass is indicative of binding which begins with the introduction of nanoparticles bearing the epitope for which the immune responses were generated. Lack of binding to orthogonal particles has been demonstrated through negative controls

designs, the antibodies were able to bind with the epitope-functionalized nanoparticles. Calculations using Spartan computational software show the spatial projection of tiopronin molecules to be about 7 Å from the gold surface, and the peptides, due to the PEG addition, extend 20 Å, from the gold surface [48]. The addition of the six-mer PEG link between the epitope and the terminal cysteine enhanced the probability for cluster–epitope interaction with antibody by distancing the epitope from the gold surface. This enhanced binding was demonstrated with both ELISA and QCM studies.

Several observations can be made by inspection of the QCM responses (Fig. 2, recorded data and schematic of adsorption) during sensor formation. Both antibodies are found to bind well to protein G. Observed spikes during assembly occur when reagent flowing through the peristaltic pump is momentarily interrupted for reactant exchange. A time delay (1–2 min) between spike and sensor response was due to the requisite transport time for the analyte to move through the peristaltic pump to the QCM sensor. The change in mass measured with the QCM is indicative of the

Table 1 Change in mass detected with the QCM for the addition of each layer of adsorbed molecules: protein G, antibodies, and epitope functionalized nanoparticles

Antibody, nanoparticle	Calculated change in mass		
	Protein G (ng)	Antibody (ng)	Nanoparticle (ng)
Anti-FLAG, FLAG-Au	100	270	30
Anti-FLAG, FLAG-Au	150	300	40
Anti-FLAG, FLAG-Au	80	270	30
Anti-HA, HA-Au	170	120	30
Anti-HA, HA-Au	60	180	50
Anti-HA, HA-Au	110	280	40
Anti-FLAG, HA-FLAG-Au	170	370	50
Anti-FLAG, HA-FLAG-Au	180	280	30
Anti-FLAG, HA-FLAG-Au	70	220	30
Anti-HA, HA-FLAG-Au	220	430	30
Anti-HA, HA-FLAG-Au	140	290	40
Anti-HA, HA-FLAG-Au	140	270	40
Negative controls			
Anti-FLAG, HA-Au	130	320	0
Anti-FLAG, HA-Au	70	260	0
Average	128	276	37[a]
Standard deviation	48	75	8[a]

Average adsorption occurred in 10 min (protein G), 16 min (antibodies), and 11 min (functionalized nanoparticles)

[a] Denotes average and standard deviation determined without including the negative controls

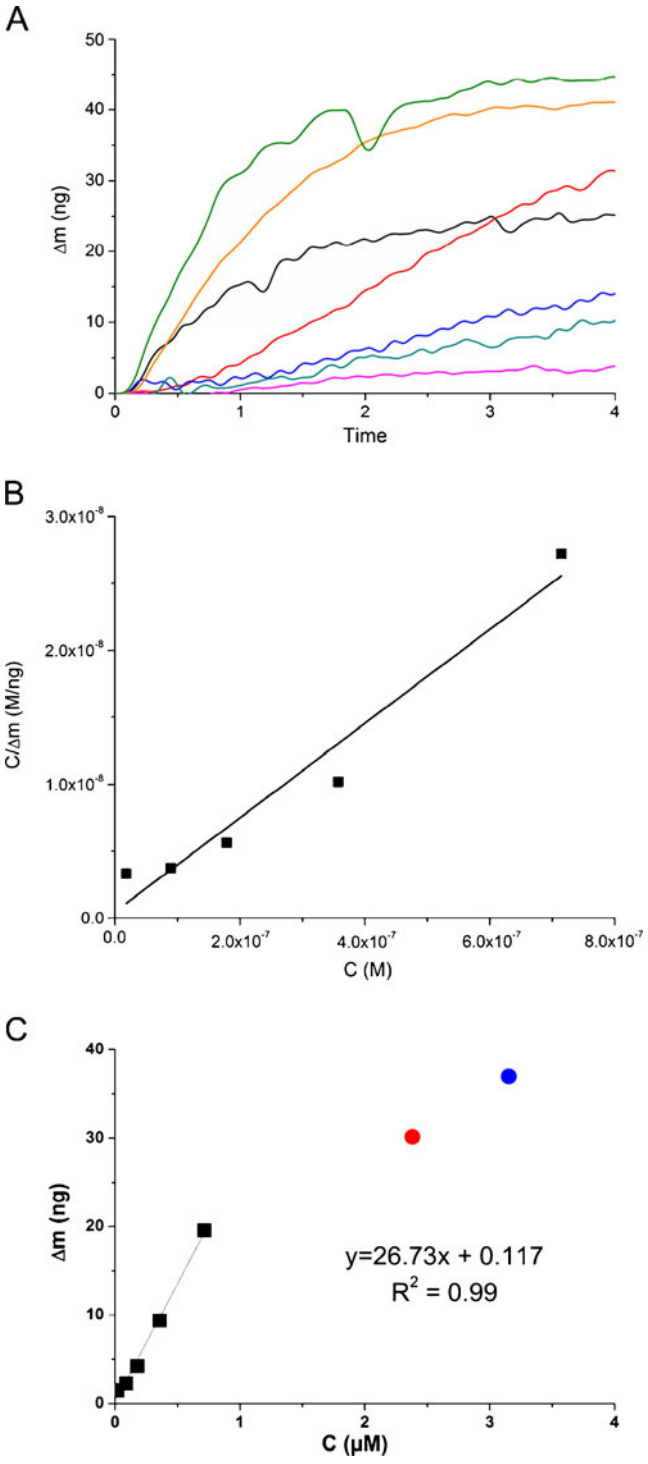

Fig. 4 Calibration of HA protein binding to anti-HA. **a** The average change in mass of H5N1 HA protein binding was determined at varying concentrations. Briefly, (*black line*) 40 μg/mL (n=2), (*red line*) 20 μg/mL (n=5), (*blue line*) 10 μg/mL (n=3), (*teal line*) 5 μg/mL (n=3), and (*pink line*) 1 μg/mL (n=4). Also shown for comparison is the binding of HA-Au (*green line*) and HA-FLAG-Au (*orange line*). **b** A linear representation of the Langmuir isotherm produced by this average binding is shown with a linear relationship of $y = (0.035 \pm 0.004)x + (4.90 \pm 15.5) \times 10^{-10}$ and R^2=0.96. **c** Calibration curve for an assay time of 1.5 min where the *black squares* are HA proteins, and the *red* and *blue dots* are HA-FLAG-Au and HA-FLAG, respectively

binding of the nanoparticles and the HA protein to the HA–antibody (Fig. 3a) and to the FLAG–antibody (Fig. 3b). Detection of the HA protein confirms the ability of this assay to detect HA specific to the H5 HA subtype, and thus the use of this HA-functionalized nanoparticle as a viral simulant. This change in mass is based on the relationship that both frequency and resistance changes have on mass load. Originally, the Sauerbrey equation was applied in air or in a vacuum, and the resulting equation was only valid for thin solid layers deposited on the resonator [49]. Since then, extensive work has been done to establish the use of the QCM to probe interactions in a liquid environment, involving suitable oscillator circuits, fluid modeling in viscous and lossy fluids, as well as determination of the relationship between motional resistance and mass load [12, 45, 50]. The sensing layers utilized in this study should yield at most a layer 30-nm thick, using liberal estimates, where the Sauerbrey equation can be applicable to thin films less than 250 nm [51–54]. Previous work, which uses a sucrose calibration, modifies the Sauerbrey equation to account for the changes that do occur in part from motional resistance, and therefore allows the ideology behind the Sauerbrey equation to apply in environments where energy is dissipated in the non-rigid liquid environment [30]. The nanoparticles increase the resistance of the crystals, and thus the rigidity, as well as decreased the frequency, resulting in a detectable increase of mass adsorbed on the surface of the crystal. Binding to the HA–antibody (positive Δm) occurs if the gold nanoparticle is functionalized with either HA or both HA and FLAG epitopes, but does not occur if the cluster is only FLAG functionalized (Fig. 3a). The nonspecific binding observed with ELISA of Au–tiopronin to anti-HA was not observed with the QCM. QCM naturally prohibits nonspecific binding through the acceleration of adhered particles. This acceleration is generated by the oscillation of the quartz and can help remove weakly bound or nonspecifically bound molecules [55, 56]. Similar binding of anti-FLAG to FLAG-Au and HA-Au-FLAG but not HA-Au was measured with the QCM (Fig. 3b). Thus, orthogonal and normalized binding at the QCM is observed consistent with immunological results obtained from ELISA, but is observable in a much shorter time interval (10 min compared to the 4 h it took to complete the ELISAs) when using the developed immunoassay and the QCM.

The demonstrated binding between bi-functionalized nanoparticles and their respective antibodies makes evident the practicality of their use as a simulant for microorganisms, while lacking the difficulties associated with use of an attenuated or killed pathogen. When a change in

mass is observed upon introduction of the functionalized MPC to the immunosensor, the immunological response is shown to be above the limit of detection (~3 ng, calculated by three times the average noise). Results show the average change in mass for protein G to be 128±48 ng, for antibodies to be 276±75 ng, and for the nanoparticle simulants to be 37±8 ng (Table 1). While the time was held constant for each step, the binding varied slightly, which could be due to slight variations in surface roughness and the surface coverage of prior adsorption steps. Even with a standard deviation of 75 ng for antibody adsorption, a deviation of only 8 ng was measured for the final detection step. The binding of the nanoparticles demonstrates saturation behavior (Fig. 3). Based on the shape of the QCM curves and the rapid increase in mass with time, it can be assumed that the kinetics would occur quickly and with presumably large equilibrium association constants. To test this theory, a calibration of anti-HA to HA binding was determined, and the binding of the functionalized nanoparticles was compared. The HA protein from H5N1 was exposed to anti-HA antibodies at concentrations ranging from 1 to 40 μg/mL (Fig. 4a, b). This binding can be compared at any time point to generate a calibration curve (Fig. 4c, example shown is at 1.5 min). Based upon the desired separation of the lower data points, the binding can continue for several more minutes. Also, the amount of nanoparticle exposed to the surface can be lowered to prevent overloading of the sensor. Measuring the maximum binding that occurs, as opposed to lower time points, can be used to determine the equilibrium association constant (K_a) and increase our understanding of the affinity of our sensor. This constant was determined by fitting to a linear rearrangement of the Langmuir adsorption isotherm, where C was plotted versus $C/\Delta m$ (Eq. 3, Fig. 4b) [30]:

$$\frac{C}{\Delta m} = \frac{1}{\Delta m_{\max}} C + \frac{1}{\Delta m_{\max} K_a}. \quad (3)$$

This yielded an equilibrium association constant for the binding between the HA protein and anti-HA of 7.14±0.26×10^7. This K_a is in the range expected for antibody–antigen interactions, from 10^6 to 10^{10} M^{-1} [57]. In fitting the binding of the nanoparticles to this Langmuir isotherm calibration (at the experimentally used nanoparticle concentration of 500 μg/mL), the sensor response to HA-FLAG-Au would have the same binding as 0.92±0.01 μM HA protein, and HA-Au would generate the same sensor response as 1.50±0.02 μM HA protein. The large response seen is at the maximum of the Langmuir isotherm. This demonstrates that even at lower concentrations, these functionalized nanoparticles can be used as a positive control. The functionalized MPC–antibody binding is not inhibited by the presence of an additional non-interacting epitope (either FLAG or HA) on the polyfunctionalized nanoparticle; therefore, multiple binding interactions can be explored simultaneously.

Conclusion

The ability to create multi-epitope-presenting nanoparticles that can orthogonally bind to specific monoclonal antibodies has been demonstrated using both ELISA and immunological QCM. Determination of the extent of antibody-functionalized nanoparticle binding is rapid using the QCM compared to ELISA. Also, like ELISA, the immunological response is specific, with QCM incurring less nonspecific binding. Interaction of the epitope with its antibody was improved through the use of a PEG linkage for epitope attachment to the MPC. Binding studies at the QCM show that polyfunctionalized gold nanoparticles exhibit the expected affinity to both antibodies that a normal immunological response is achieved from matched antibody–antigen couples and that an orthogonal response results otherwise. The results demonstrate that binding of polyfunctionalized gold nanoparticles could be used to determine sensor functionality, without resorting to the use of attenuated or killed microorganisms, or extracted and purified whole proteins.

Acknowledgements The authors acknowledge support from NIH grant R01 GM076479 and DTRA HDTRA1-10-0067. Leslie A. Hiatt acknowledges support from a Department of Education GAANN fellowship (P200A040022). Robert G. Keil acknowledges sabbatical leave support received from the University of Dayton and Vanderbilt University. We thank Brian N. Turner for his assistance in TEM and TGA data collection.

References

1. Acheson NH (2007) Fundamentals of molecular virology. Wiley, Hoboken, pp 248–260
2. Ferguson NM, Fraser C, Donnelly CA, Ghani AC, Anderson RM (2004) Science 304:968–969
3. Wilson IA, Niman HL, Houghten RA, Cherenson AR, Connolly ML, Lerner RA (1984) Cell 37:767–778
4. Gerdon AE, Wright DW, Cliffel DE (2005) Biomacromolecules 6:3419–3424
5. Rutledge RD, Huffman BJ, Cliffel DE, Wright DW (2008) J Mater Res 23:3161–3168
6. Wittenberg NJ, Haynes CL (2009) Wiley Interdiscip Rev Nanomed Nanobiotechnol 1:237–254
7. Mackiewicz MR, Hodges HL, Reed SM (2010) J Phys Chem B 114:5556–5562
8. Smith S (2009) BU grad student develops infection: possible link to lab experiments raises new safety concerns. The Boston Globe [Online], 30 Oct 2009. Available at http://www.boston.com/news/health/articles/2009/10/30/bu_grad_student_develops_infection/. Accessed 23 Sep 2010

9. Mani V, Chikkaveeraiah BV, Patel V, Gutkind JS, Rusling JF (2009) ACS Nano 3:585–594
10. Xia H, Wang F, Huang Q, Huang J, Chen M, Wang J, Yao C, Chen Q, Cai G, Fu W (2008) Sensors 8:6453–6470
11. Zuo B, Li S, Guo Z, Zhang J, Chen C (2004) Anal Chem 76:3536–3540
12. Skottrup PD, Nicolaisen M, Justesen AF (2008) Biosens Bioelectron 24:339–348
13. Peduru Hewa TM, Tannock GA, Mainwaring DE, Harrison S, Fecondo JV (2009) J Virol Methods 162:14–21
14. Nam J-M, Thaxton CS, Mirkin CA (2003) Science 301:1884–1886
15. Tang DP, Yuan R, Chai YQ, Zhong X, Dai JY, Zhang LY (2004) Anal Biochem 333:345–350
16. Ho K-C, Tsai P-J, Lin Y-S, Chen Y-C (2004) Anal Chem 76:7162–7168
17. Liu G, Wang J, Kim J, Jan MR (2004) Anal Chem 76:7126–7130
18. Ingram RS, Hosteller MJ, Murray RW (1997) J Am Chem Soc 119:9175–9178
19. Agasti SS, Rana S, Park M-H, Kim CK, You C-C, Rotello VM (2010) Adv Drug Delivery Rev 62:316–328
20. Sardar R, Funston AM, Mulvaney P, Murray RW (2009) Langmuir 25:13840–13851
21. Shangguan T, Siegel DP, Lear JD, Axelsen PH, Alford D, Bentz J (1998) Biophys J 74:54–62
22. Bowman M-C, Ballard TE, Ackerson CJ, Feldheim DL, Margolis DM, Melander C (2008) J Am Chem Soc 130:6896–6897
23. Montet X, Funovics M, Montet-Abou K, Weissleder R, Josephson L (2006) J Med Chem 49:6087–6093
24. Wegner GJ, Lee HJ, Corn RM (2002) Anal Chem 74:5161–5168
25. Muller GM, Shapira M (1982) Proc Natl Acad Sci USA 79:569–573
26. Lu Y, Ding J, Chen Y-H (2002) Int Arch Allergy Immunol 127:245–250
27. Brauer G (1965) Handbook of preparative inorganic chemistry, vol 2. Academic, New York, pp 1053–1056
28. Nwe N, He Q, Damrongwatanapokin S, Du Q, Manopo I, Limlamthong Y, Fenner B, Spencer L, Kwang J (2006) BMC Microbiology 6:16
29. Templeton AC, Cliffel DE, Murray RW (1999) J Am Chem Soc 120:4845–4849
30. Gerdon AE, Wright DW, Cliffel DW (2005) Anal Chem 77:304–310
31. Templeton AC, Chen S, Gross SM, Murray RW (1999) Langmuir 15:66–76
32. Gerdon AE, Wright DW, Cliffel DE (2005) Quartz crystal microbalance characterization of nanostructure assemblies in biosensing. In: Kumar C (ed) Characterization tools for nanosystems in life sciences, vol 3. Wiley-VCH, New York, pp 109–144
33. Hostetler MJ, Wingate JE, Zhong C-J, Harris JE, Vachet RW, Clark MR, Londono JD, Green ST, Stokes JJ, Wignall GD (1998) Langmuir 14:17–30
34. Simpson CA, Huffman BJ, Gerdon AE, Cliffel DE (2010) Chem Res Toxicol 23:1608–1616
35. Chan WC, White PD (2000) Fmoc solid phase peptide synthesis, The practical approach series. Oxford University Press, New York, pp 9–74
36. Lloyd-Williams P, Albericio F, Giralt E (1997) Chemical approaches to the synthesis of peptides and proteins. CRC, New York, pp 12–16
37. Van Regenmortel MHV (1989) Phil Trans R Soc B 323:451–466
38. Hostetler MJ, Templeton AC, Murray RW (1999) Langmuir 15:3782–3789
39. Montalti M, Prodi L, Zaccheroni N, Baxter R, Teobaldi G, Zerbetto F (2003) Langmuir 19:5172–5174
40. Jadzinsky PD, Calero G, Ackerson CJ, Bushnell DA, Kornberg RD (2007) Science 318:430–433
41. Buttry DA (1991) Applications of the QCM to electrochemistry. In: Bard AJ (ed) Electroanalytical chemistry: a series of advances, vol 17. Marcel Dekker, New York, p 10
42. Tsionsky V, Daikhin L, Urbakh M, Gileadi E (2004) Theoretical interpretation of the QCM response. In: Bard AJ, Rubinstein I (eds) Electroanalytical chemistry: a series of advances, vol 22. Marcel Dekker, New York, pp 8–26
43. Kanazawa KK, Gordon JG (1985) Anal Chem 57:1771–1772
44. Martin SE, Granstaff V, Frye G (1991) Anal Chem 63:2272–2281
45. Kanazawa KK (1997) Faraday Discuss 107:77–90
46. Harkness KM, Fenn LS, Cliffel DE, McLean JA (2010) Anal Chem 82:3061–3066
47. Steinitz M (2000) Anal Biochem 282:232–238
48. Hehre WH (2005) Spartan '04. Wavefunction, Inc., Irvine
49. Sauerbrey G (1959) Zeitschrift fuer Physik 155:206–222
50. Cooper MA, Singleton VT (2007) J Mol Recognit 20:154–184
51. Sauer-Eriksson AE, Kleywegt GJ, Uhlen M, Jones TA (1995) Structure 3:265–278
52. Yang L, Biswas ME, Chen P (2003) Biophys J 84:509–522
53. Labrijn AF, Poignard P, Raja A, Zwick MB, Delgado K, Franti M, Binley J, Vivona V, Grundner C, Huang C-C, Venturi M, Petropoulos CJ, Wrin T, Dimitrov DS, Robinson J, Kwong PD, Wyatt RT, Sodroski J, Burton DR (2003) J Virol 77:10557–10565
54. Su X-L, Li Y (2005) Biosens Bioelectron 21:840–848
55. Hirst ER, Yuan YJ, Xu WL, Bronlund JE (2008) Biosens Bioelectron 23:1759–1768
56. Cooper MA (2003) Meas Sci Technol 14:1888–1893
57. Nelson DL, Cox MM (2000) Lehninger principles of biochemistry, 3rd edn. Worth, New York, pp 228–232